SOLUTION OF THE EULER EQUATIONS FOR TWO DIMENSIONAL TRANSONIC FLOW BY A MULTIGRID METHOD *

Antony Jameson
Princeton University
Princeton, NJ 08544

1 Introduction

A crucial input to the design of a long range aircraft is the prediction of the aerodynamic flow in cruising flight. In contrast to the flow past a blunt object, such as a golf ball, or ski racer, the flow past an aircraft generally does not separate. Consequently, the important viscous effects are mainly confined to boundary layers over the surface of the aircraft, and useful predictions can be made by solving the equations of inviscid flow. The cruising efficiency is roughly proportional to the speed multiplied by the lift to drag ratio, so that it pays to increase the speed into the transonic range, where compressibility effects lead to the formation of shock waves, and have a dominating influence on the flow.

During the last decade, numerous codes have been developed for the solution of the potential flow equation in transonic flow. Some of these codes employ sophisticated numerical algorithms, and are capable of treating flows in complex geometric domains [1,2]. It has been established that the multigrid technique can dramatically accelerate the convergence of transonic potential flow calculations,although the governing equations are of mixed elliptic and hyperbolic type [3-6].

The assumption of potential flow implies that the flow is irrotational. This is not strictly correct when shock waves are present. An exact description of transonic inviscid flow requires the solution of the Euler equations. The numerical solution of the Euler equations for steady transonic flows is therefore a problem of great interest to the aeronautical community. It also presents a testing challenge to applied mathematicians and numerical analysts.

A variety of implicit and explicit schemes have recently been developed for the solution of the Euler equations [7-12]. The multistage explicit scheme proposed by Jameson, Schmidt and Turkel [11] has proved to be one of the most efficient, and it is presently being applied to calculate the flow past a wing-body-tail-fin combination [12]. A novel multigrid scheme for the solution of the Euler equations was proposed by Ni [13]. Ni obtained a convergence rate of about .95, measured by the mean error reduction per multigrid cycle. In its published form his scheme includes an artificial dissipative term which restricts the results to first order accuracy. In this paper it is shown that the multistage time stepping scheme can be adapted for use in conjunction with a multigrid technique to produce a rapidly convergent algorithm for calculating steady state solutions of the Euler equations.

*Reprinted from Applied Mathematics and Computation 13:327-355(1983), NY, 1983

2 Formulation of the Equations and Space Discretization

The underlying idea of the multistage scheme is to separate the procedures for space and time discretization. The space discretization yields a set of coupled ordinary differential equations which can be solved by a multistage time stepping scheme. The reformulation of the time stepping scheme for use with multiple grids preserves the same steady state solution.

The space discretization scheme is developed by expressing the Euler equations in integral form. Let p, ρ, u, v, E and H denote the pressure, density, Cartesian velocity components, total energy and total enthalpy. For a pefect gas

$$E = \frac{p}{(\gamma - 1)} + \frac{1}{2}(u^2 + v^2), H = E + \frac{p}{\rho} \tag{2.1}$$

where γ is the ratio of specific heats. The Euler equations can be written as

$$\frac{\partial}{\partial t} \int \int_S w dS + \int_{\partial S} (f dy - g dx) = 0 \tag{2.2}$$

for a domain S with boundary ∂S. Here w represents the conserved quantities, and f and g are the fluxes in x and y directions:

$$w = \begin{pmatrix} \rho \\ \rho u \\ \rho v \\ \rho E \end{pmatrix}, f = \begin{pmatrix} \rho u \\ \rho u^2 + p \\ \rho uv \\ \rho uH \end{pmatrix}, g = \begin{pmatrix} \rho v \\ \rho vu \\ \rho v^2 + p \\ \rho vH \end{pmatrix} \tag{2.3}$$

The computational domain is divided into quadrilateral cells denoted by the subscripts i,j, as sketched in Figure 1. Assuming that the dependent variables are known at the center of each cell, a system of ordinary differential equations is obtained by applying equation (2) separately to each cell. These have the form

$$\frac{d}{dt}(S_{ij} w_{ij}) + Q_{ij} = 0 \tag{2.4}$$

where S_{ij} is the cell area, and Q_{ij} is the net flux out of the cell. The flux for the x momentum component, for example is

$$\sum_{k=1}^{4} q_k (\rho u)_k + \Delta y_k p_k \tag{2.5}$$

where q_k is the flux velocity

$$q_k = \Delta y_k u_k - \Delta x_k v_k \tag{2.6}$$

and the sum is over the four sides of the cell. Each quantity is evaluated as the average of the values in the cells on either side of the edge:

$$(\rho u)_1 = \frac{1}{2}\{(\rho u)_{i,j} + (\rho u)_{i,j-1}\} \tag{2.7}$$

for example. The scheme reduces to a central difference scheme on a Cartesian grid, and is second order accurate provided that the mesh is smooth enough.

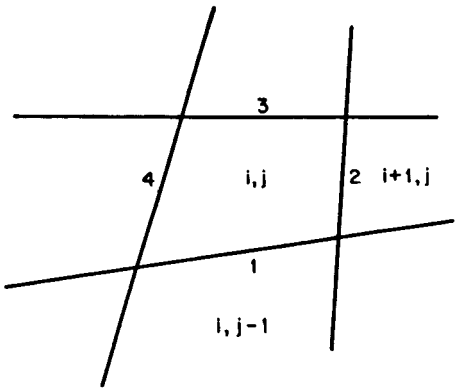

Figure 1: Discretization in Space

In order to suppress the tendency for odd and even point oscillations, and to limit overshoots near shock waves, the scheme is augmented by a dissipative term so that equation (4) becomes

$$\frac{d}{dt}(S_{ij}w_{ij}) + Q_{ij} - D_{ij} = 0 \tag{2.8}$$

Here D_{ij} is the dissipation, which is constructed so that it is of third order in smooth regions of the flow. For the density equation $D_{ij}(\rho)$ has the form

$$d_{i+\frac{1}{2},j} - d_{i-\frac{1}{2},j} + d_{i,j+\frac{1}{2}} - d_{i,j-\frac{1}{2}} \tag{2.9}$$

where

$$d_{i+\frac{1}{2},j} = \varepsilon^{(2)}_{i+\frac{1}{2},j}(\rho_{i+1,j} - \rho_{i,j}) + \varepsilon^{(4)}_{i+\frac{1}{2},j}(\rho_{i+2,j} - 3\rho_{i+1,j} + 3\rho_{i,j} - \rho_{i-1,j}) \tag{2.10}$$

Both coefficients include a normalizing factor proportional to the length of the cell side, and $\varepsilon^{(2)}_{i+\frac{1}{2},j}$ is also made proportional to the normalized second difference of the pressure

$$\nu_{ij} = \left| \frac{p_{i+1,j} - 2p_{i,j} + p_{i-1,j}}{p_{i+1,j} + 2p_{i,j} + p_{i-1,j}} \right| \tag{2.11}$$

in the adjacent cells. This quantity is of second order except in regions containing a steep pressure gradient. The fourth differences provide background dissipation throughout the domain. In the neighborhood of a shock wave, however, ν_{ij} is of order 1, and the second differences become the dominant dissipative terms. The dissipative terms for the other equations are constructed from similar formulas, except that in the energy equation the differences are of ρH rather than ρE. The purpose of this is to allow a steady state solution for which H remains constant.

At a solid boundary the only contribution to the flux balance (5) comes from the pressure. The normal pressure gradient $\frac{\partial p}{\partial n}$ at the wall can be estimated from the condition that $\frac{\partial}{\partial t}(\rho q_n)$, where q_n is the normal velocity component. The pressure at the wall is then estimated by extrapolation from the pressure at the adjacent cell centers, using the known value of $\frac{\partial p}{\partial n}$.

The rate of convergence to a steady state will be impaired if outgoing waves are reflected back into the flow from the outer boundaries. The treatment of the far field boundary condition is based on the introduction of Riemann invariants for a one dimensional flow normal to the boundary. Let subscripts ∞ and e denote free

stream values, and values extrapolated from the interior cells adjacent to the boundary, and let q_n and c be the velocity component normal to the boundary and the speed of sound. Assuming that the flow is subsonic at infinity, we introduce fixed and extrapolated Riemann invariants.

$$R_\infty = q_{n_\infty} - \frac{2c_\infty}{\gamma - 1}$$

and

$$R_e = q_{n_e} + \frac{2c_e}{\gamma - 1}$$

corresponding to incoming and outgoing waves. These may be added and subtracted to give

$$q_n = \frac{1}{2}(R_e + R_\infty)$$

and

$$c = \frac{\gamma - 1}{4}(R_e - R_\infty)$$

where q_n and c are the actual normal velocity component and speed of sound to be specified in the far field. At an outflow boundary, the tangential velocity component and entropy are extrapolated from the interior, while at an inflow boundary they are specified as having free stream values. These four quantities provide a complete definition of the flow in the far field. If the flow is supersonic in the far field, all the flow quantities are specified at an inflow boundary, and they are extrapolated from the interior at an outflow boundary.

3 Multistage Time Stepping Scheme

In the numerical solution of ordinary differential equations multistage schemes are usually designed to give a high order of accuracy. Since the present objective is simply to obtain a steady state as rapidly as possible, the order of accuracy is not important. This allows the use of simplified schemes selected purely for their properties of stability and damping.

Since the cell area S_{ij} is independent of time, equation (8) can be written as

$$\frac{dw}{dt} + R(w) = 0 \tag{3.12}$$

where $R(w)$ is the residual

$$R_{ij} = \frac{1}{S_{ij}}(Q_{ij} - D_{ij})$$

A class of k stage schemes to advance equation (12) by a time step Δt can be written as

$$\begin{aligned} w^{(0)} &= w^n \\ w^{(1)} &= w^{(0)} - \alpha_1 \Delta t R^{(0)} \\ &\cdots \\ w^{(k-1)} &= w^{(0)} - \alpha_{k-1} \Delta t R^{(k-2)} \\ w^{(k)} &= w^{(0)} - \Delta t R^{(k-1)} \\ w^{n+1} &= w^{(k)} \end{aligned} \tag{3.13}$$

where w^n and w^{n+1} are the values at the beginning and end of the n^{th} time step. In a conventional scheme the residual the $(q-1)^{st}$ stage would be evaluated as

$$R^{(q)} = \frac{1}{S_{ij}}\left(Q_{ij}(w^{(q)}) - D_{ij}(w^{(q)})\right) \tag{3.14}$$

A substantial saving in computational effort can be realized, however, by freezing the dissipative part at its value at the first stage. The residual in the $(q+1)^{st}$ stage is then evaluated as

$$R^{(q)} = \frac{1}{S_{ij}}\left(Q_{ij}(w^{(q)}) - D_{ij}(w^{(0)})\right) \tag{3.15}$$

In order to assess the properties of these schemes it is useful to consider the model problem

$$u_t + u_x + \mu\Delta x^3 u_{xxx} = 0 \tag{3.16}$$

In the absence of the third order dissipative term this equation describes the propagation of a disturbance without distortion at unit speed. With centered differences the residual has the form

$$\Delta t R(u)_i = \lambda(u_{i+1} - u_{i-1}) + \lambda\mu(u_{i+2} - 4u_{i+1} + 6u_i - 4u_{i-1} + u_{i-2})$$

where $\lambda = \Delta t/\Delta x$ is the Courant number.

If we consider a Fourier mode $\hat{u} = e^{ipx}$ the discretization in space yields

$$\frac{d\hat{u}}{dt} = z\hat{u}$$

where z is the Fourier symbol of the residual

$$z = -\lambda i \sin\xi - \lambda\mu(1 - \cos\xi)^2$$

A single step of the multistage scheme yields

$$\hat{u}^{n+1} = g(z)\hat{u}^n$$

where g(z) is the amplification factor. The stability region of the scheme given by those values of z for which $g(z) \leq 1$.

An efficient 4 stage scheme, which is also fourth order accurate for the linear problem, is given by the coefficient values

$$\alpha_1 = 1/4, \alpha_2 = 1/3, \alpha_3 = 1 \tag{3.17}$$

If the dissipative terms are reevaluated at each stage (equation (14)), the amplification factor is given by the polynomial

$$g(z) = 1 + z + \frac{z^2}{2} + \frac{z^3}{6} + \frac{z^4}{24}$$

The stability region of this scheme is shown in Figure 2, which displays contour lines for $|g| = 1, .9, .8, \ldots$ The Figure also shows the locus of z as the wave number is varied between 0 and 2π for a Courant number $\lambda = 2.8$, and a dissipation coefficient $\mu = 1/32$. The corresponding variation of $|g|$ with ξ is shown in Figure 3. The intercept of the stability region with the imaginary axis is $2\sqrt{2}$. The corresponding bound on the time step is $\Delta t \leq \Delta x/2\sqrt{2}$ .It can be shown that in the absence of dissipation this is the maximum attainable with a four stage scheme [14]. If the same coefficients are used, but the dissipative terms are evaluated only once (equation (15)), the stability region assumes the form shown in Figure 3. This also shows that this form of the scheme is stable for a Courant number of 2.6 with the same amount of dissipation.

Numerical experiments have confirmed the stability and efficiency of these schemes for the solution of the Euler equations [11,12]. The slight reduction in the time step which is required when the dissipative terms are only evaluated once in each time step is more than compensated by the saving in computational effort. In calculations on a single grid the best rate of convergence generally seems to be obtained by choosing the coefficients to maximize the time step. This leads to the most rapid expulsion of disturbances through the outer boundary.

4 Multigrid Scheme

While the available theorems in the theory of multigrid methods generally assume ellipticity, it seems that it ought to be possible to accelerate the evolution of a hyperbolic system to a steady state by using large time steps on coarse grids, so that disturbances will be more rapidly expelled through the outer boundary. The interpolation of corrections back to the fine grid will introduce errors, however, which cannot be rapidly expelled from the fine grid, and ought to be locally damped, if a fast rate of convergence is to be attained. Thus it remains important that the driving scheme should have the property of rapidly damping out high frequency modes.

In order to adapt the multistage scheme for a multigrid algorithm, auxiliary meshes are introduced by doubling the mesh spacing. Values of the flow variables are transferred to a coarser grid by the rule

$$w_{2h}^{(0)} = \sum S_h w_h / S_{2h} \tag{4.18}$$

where the subscripts denote values of the mesh spacing parameter, S is the cell area, and the sum is over the u cells on the fine grid composing each cell on the coarse grid. This rule conserves mass, momentum and energy. A forcing function is then defined as

$$P_{2h} = \sum R_h(w_h) - R_{2h}(w_{2h}^{(0)}) \tag{4.19}$$

where R is the residual of the difference scheme. In order to update the solution on a coarse grid, the multistage scheme (13) is reformulated as

$$\begin{aligned} w^{(1)} &= w_{2h}^{(0)} - \alpha_1 \Delta t (R_{2h}^{(0)} + P_{2h}) \\ &\cdots \\ w_{2h}^{(q+1)} &= w_{2h}^{(0)} - \alpha_q \Delta t (R_{2h}^{(0)} + P_{2h}) \\ &\cdots \end{aligned} \tag{4.20}$$

where $R^{(q)}$ is the residual at the q^{th} stage. In the first stage of the scheme, the addition of P_{2h} cancels $R_{2h}(W_{2h}^{(0)}))$ and replaces it by $\sum R_h(w_h)$, with the result that the evolution on the coarse grid is driven by the residuals on the fine grid. This process is repeated on successively coarser grids. Finally the correction calculated on each grid is passed back to the next finer grid by bilinear interpolation.

Since the evolution on a coarse grid is driven by residuals collected from the next finer grid, the final solution on the fine grid is independent of the choice of boundary conditions on the coarse grids. The surface boundary condition is treated in the same way on every grid, by using the normal pressure gradient to extrapolate the surface pressure from the pressure in the cells adjacent to the wall. The far field conditions can either be transferred from the fine grid, or recalculated by the procedure described in Section 2.

In multigrid calculations it is more important to improve the damping of high frequency modes than it is to maximize the time step. When the four stage scheme (20) is used with a single evaluation of the dissipate terms (equation (15)), a good choice of the coefficients is

(4.21) $$\alpha_1 = .25, \alpha_2 = .5, \alpha_3 = .55$$

The resulting stability region for the model problem (16) is shown in Figure 6. From Figure 7 it can also be seen that with a Courant number $\lambda = 2.0$ and a dissipation coefficient $\mu = 1/32$, the magnitude of $|g|$ of the amplification factor is less than .35 for all wave numbers in the range $1.0 < \xi < \pi$

It turns out that an effective multigrid strategy is to use a simple saw tooth cycle (as illustrated in Figure 8), in which a transfer is made from each grid to the next coarser grid after a single time step. After reaching the coarsest grid the corrections are then successively interpolated back from each grid to the next finer grid without any intermediate Euler calculations. On each grid the time step is varied locally to yield a fixed Courant number, and the same Courant number is generally used on all grids, so that progressively larger time steps are used after each transfer to a coarser grid. In comparison with a single time step of the Euler scheme on the fine grid, the total computational effort in one multigrid cycle is

$$1 + \frac{1}{4} + \frac{1}{16} + \ldots \leq \frac{4}{3}$$

plus the additional work of calculating the forcing functions P, and interpolating the corrections.

5 Enthalpy Damping

Provided that the enthalpy has a constant value H_∞ in the far field, it is constant everywhere in a steady flow, as can be seen by comparing the equations for conservation of mass and energy. If we set $H = H_\infty$ everywhere in the flow field throughout the evolution, then the pressure can be calculated from the equation

$$p = \frac{\gamma - 1}{\gamma}\rho(H_\infty - \frac{u^2 + v^2}{2})$$

This eliminates the need to integrate the energy equation. The resulting three equation model still constitutes a hyperbolic system, which approaches the same steady state as the original system.

An alternative modification is to retain the energy equation, and to add forcing terms proportional to the difference between H and H_∞ [15]. Since the space discretization scheme of Section 2 is constructed in such a way that $H = H_\infty$ is consistent with the steady state solution of the difference equations, these terms do not alter the final steady state. Numerical experiments have confirmed that they do assist convergence. The terms added to the mass and momentum equations are $\alpha\rho(H - H_\infty), \alpha\rho u(H - H_\infty)$ and $\alpha\rho v(H - H_\infty)$, while that added to the energy equation is $\alpha(H - H_\infty)$. In multigrid calculations an effective strategy is to include these terms only on the fine grid, and to increase the parameter α.

6 Results

A variety of two dimensional calculations have been performed to test the multigrid scheme. Figures 6-8 show results for the NACA 0012 airfoil. These calculations were performed on an 0 mesh with 128 intervals around the profile, and 32 intervals in the normal direction. The mesh is shown in Figure 9. Figure 10 shows the result for Mach .80 and zero angle of attack, while Figures 11 and 12 show the convergence rates for the four stage scheme on a single grid and with multiple grids. Each figure shows two curves. One is the decay of the logarithm of the error (measured by the root mean square rate of change of density on the fine grid). The other is the build up of the number of points in the supersonic zone. Provided that the flow is transonic, this is a useful measure of the global convergence of the flow field. The multistage scheme with a single evaluation of dissipation (equation 15), was used in both cases. The coefficients were specified by equation (17) for the calculation on a

single grid, and equation (21) for the multigrid calculation, which was performed with 5 grid levels. Although the multigrid scheme requires more work in each cycle, this cost is by far outweighed by the improvement in the rate of convergence. With the multigrid scheme the flow field is fully converged in less than 100 cycles, starting from a uniform flow. Measured by the mean error reduction per cycle, the rate of convergence for the first 100 cycles is about .9. Figure 8 shows a similar comparison for a subsonic flow at Mach .500, and an angle of attack of 3 . The rate of convergence realized by the multigrid scheme is about the same as for the transonic nonlifting flow. Figure 9 shows the solution and convergence rates for transonic flow past a circular cylinder, at Mach .45. The improvement in the convergence rate due to the introduction of multiple grids is roughly the same as for the case of the NACA 0012 airfoil.

These results clearly demonstrate that the convergence of a time dependent hyperbolic system to a steady state can be substantially accelerated by the introduction of multiple grids. With the formulation here proposed, the steady state is entirely determined by the space discretization scheme on the fine grid. It is independent of both the time stepping scheme, and the discretization procedure used on the coarse grids. Either of these could be modified in any way which would improve the rate of convergence or reduce the computational effort. The existing scheme exhibits a good shock capturing capability, and its discretization error is of second order in smooth regions of the flow. It also permits vectorization with a vector length equal to the number of cells on any given grid.

Acknowledgement

This work has benefited from the support of both the Office of Naval Research, under Grant N00014-81-K-0379 and the NASA Langley Research Center, under Grant NAG-1-186

References

[1] Jameson, Antony, *"Remarks on the Calculation of Transonic Potential Flow by a Finite Volume Method"*, Proc. IMA Conference on Numerical Methods in Fluid Dynamics, Reading, 1978, edited by B. Hunt, Academic Press, pp. 363-386.

[2] Bristeau, M. 0., Pironneau, 0., Glowinski, R., Periaux, J., Perrier, P. and Poirier, G., *"Application of Optimal Control and Finite Element Methods to the Calculation of Transonic Flows and Incompressible Viscous Flows"*,Proc. IMA Conference on Numerical Methods in Fluid Dynamics, Reading, 1978, edited by B. Hunt, Academic Press, 1980, pp. 203-212.

[3] South, J. C., and Brandt, A., *"Application of a Multi-Level Grid Method to Transonic Flow Calculations"*. Proc. of Workshop on Transonic Flow Problems in Turbomachinery, Monterey, 1976, edited by T. C. Adamson and M. F. Platzer, Hemisphere, 1977, pp. 180-206.

[4] Jameson, Antony, *"Acceleration of Transonic Potential Flow Calculations on Arbitrary Meshes by the Multiple Grid Method"*, Proc. AIAA 4th Computational Fluid Dynamics Conference, Williamsburg, 1979, pp. 122-146.

[5] McCarthy, D. R. and Reyhner, T.A., *"Multigrid Code for Three Dimensional Transonic Potential Flow About Inlets"*, AIAA Journal, 20, 1982, pp. 45-50

[6] Caughey, D. A., *"Multigrid Calculation of Three Dimensional Transonic Potential Flows"*, AIAA Paper 83-0374, 1983.

[7] Steger, J. L., *"Implicit Finite Difference Simulation of Flow About Arbitrary Two Dimensional Geometries"*, J. Computational Physics, 16, 1978, pp. 679-686.

[8] Pulliam, T., Jespersen, D., and Childs, R., *"An Enhanced Version of an Implicit Code for the Euler Equations"*, AIAA Paper 83-0344, 1983.

[9] MacCormack, R. W., *"A Numerical Method for Solving the Equations of Compressible Viscous Flows"*, AIAA Paper 81-110, 1981.

[10] Lerat, A., Sides, J., and Daru, V., *"An Implicit Finite Volume Scheme for Solving the Euler Equations"*, Proc. 8th International Conference on Numerical Methods in Fluid Dynamics, Aachen, 1982, edited by E. Krause, Springer, 1982, pp. 343-349.

[11] Jameson, A., Schmidt, W., and Turkel, E., *"Numerical Solution of the Euler Equations by Finite Volume Methods Using Runge-Kutta Time Stepping Schemes"*, AIAA Paper 81-1259, 1981.

[12] Jameson, Antony, and Baker, T. J., *"Solution of the Euler Equations for Complex Configurations"*, AIAA Paper 83-1929, 1983.

[13] Ni, R. H., *"A Multiple Grid Scheme for Solving the Euler Equations"*, Proc. AIAA 5th Computational Fluid Dynamics Conference, Palo Alto, 1981, pp. 257-264.

[14] Van der Houwen, P. J., *"Construction of Integration Formulas for Initial Value Problems"*, North Holland, 1977.

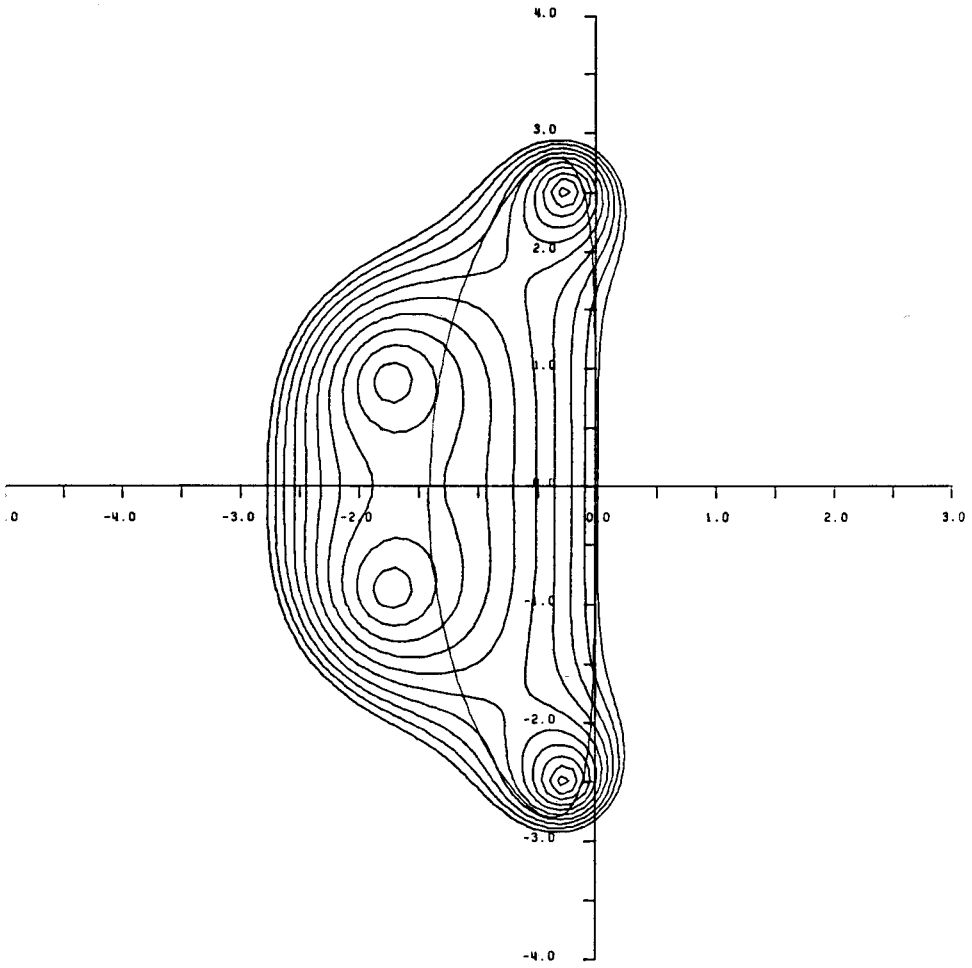

Figure 2: Stability Region of Standard 4 Stage Scheme Contour lines $|g| = 1., .8, .0, \ldots$ plus locus of $z(\xi)$ for $\lambda = 2.8, \mu = 1/32$ Coefficients of $\alpha_1 = 1/4, \alpha_2 = 1/3, \alpha_3 = 1/2$

[15] Jameson, Antony, *"Steady State Solution of the Euler Equations for Transonic Flow"*, Proc. Symposium on Transonic, Shock,, and Multidimensional Flows, Madison, 1980, edited by R. E: Meyer, Academic Press, 1982, pp. 37-70.

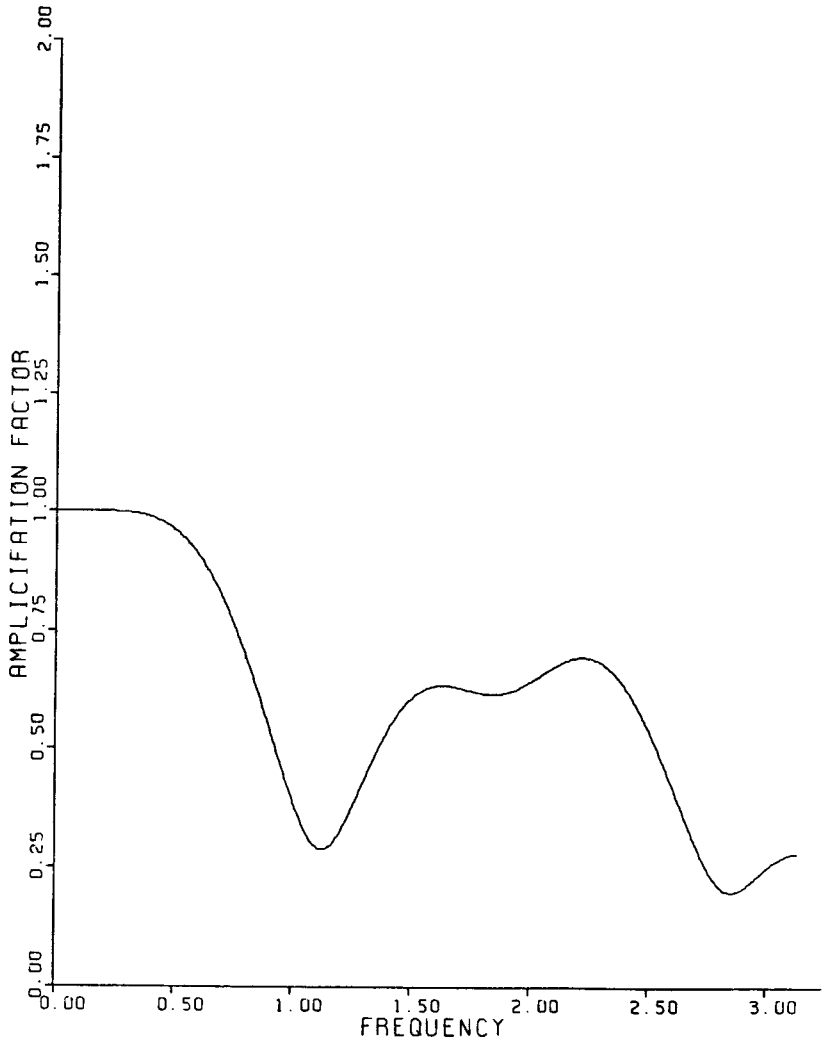

Figure 3: Amplification Factor $|g|$ of Standard 4 Stage Scheme for $\lambda = 2.8, \mu = 1/32$ Coefficients of $\alpha_1 = 1/4, \alpha_2 = 1/3, \alpha_3 = 1/2$

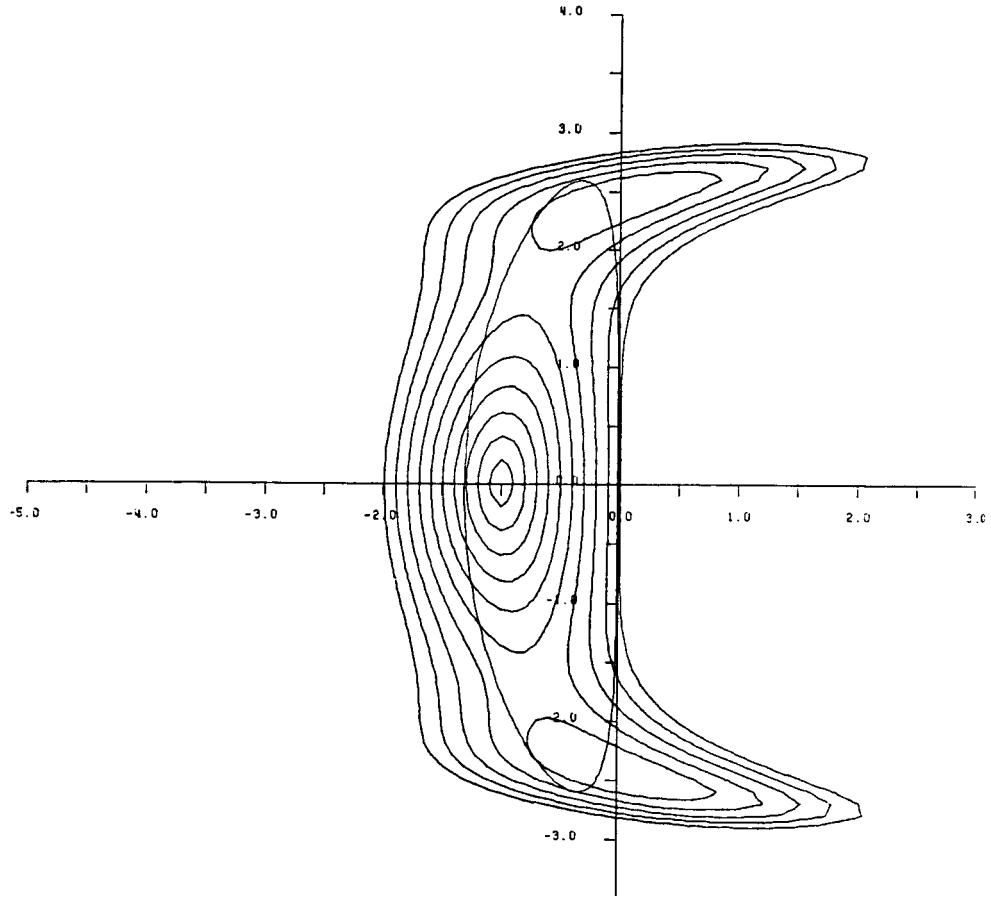

Figure 4: Stability Region of 4 Stage Scheme with Single Evaluation of Dissipation Contour lines $|g| = 1., .9., 8, \ldots$ plus locus of $z(\xi)$ for $\lambda = 2.6, \mu = 1/32$ Coefficients of $\alpha_1 = 1/4, \alpha_2 = 1/3, \alpha_3 = 1/2$

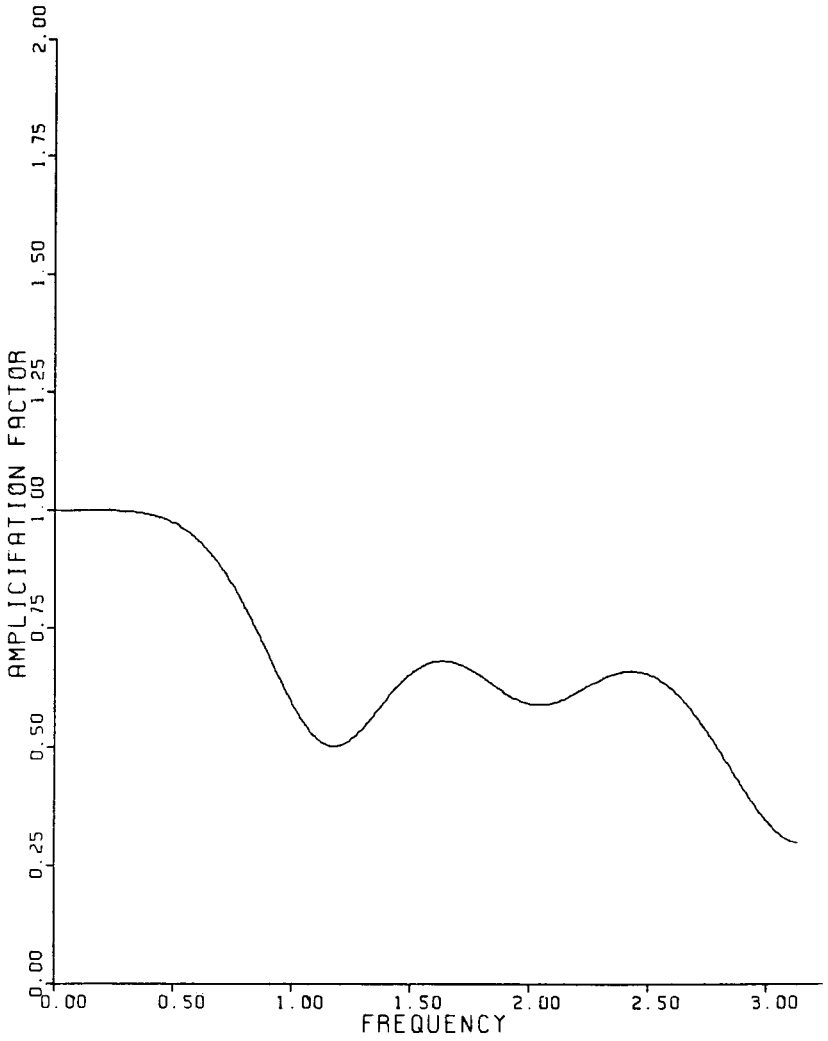

Figure 5: Amplification Factor $|g|$ of Standard 4 Stage with Single Evaluation of Dissipation for $\lambda = 2.6, \mu = 1/32$ Coefficients of $\alpha_1 = 1/4, \alpha_2 = 1/3, \alpha_3 = 1/2$

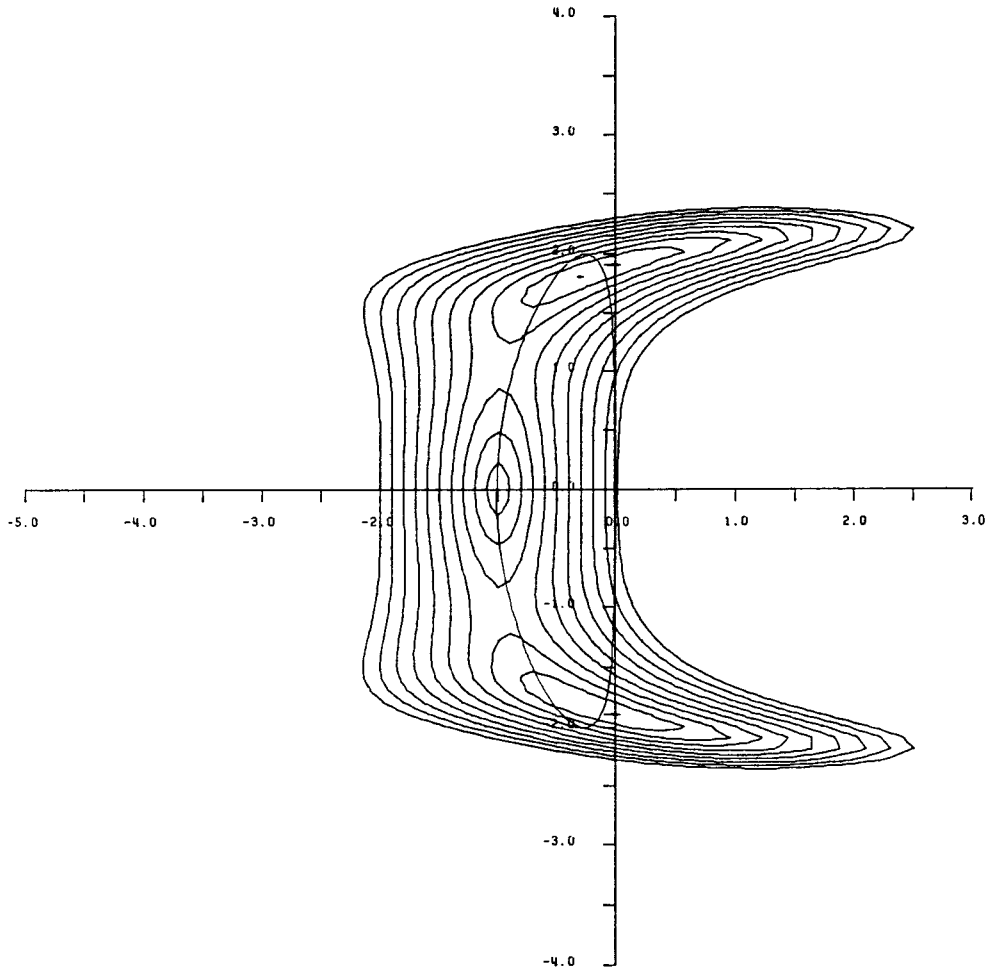

Figure 6: Stability Region of 4 Stage Scheme with Single Evaluation of Dissipation and Modified Coefficients Contour lines $|g| = 1., .9., 8, \ldots$ plus locus of $z(\xi)$ for $\lambda = 2, \mu = 1/32$ Coefficients of $\alpha_1 = .25, \alpha_2 = .5, \alpha_3 = .55$

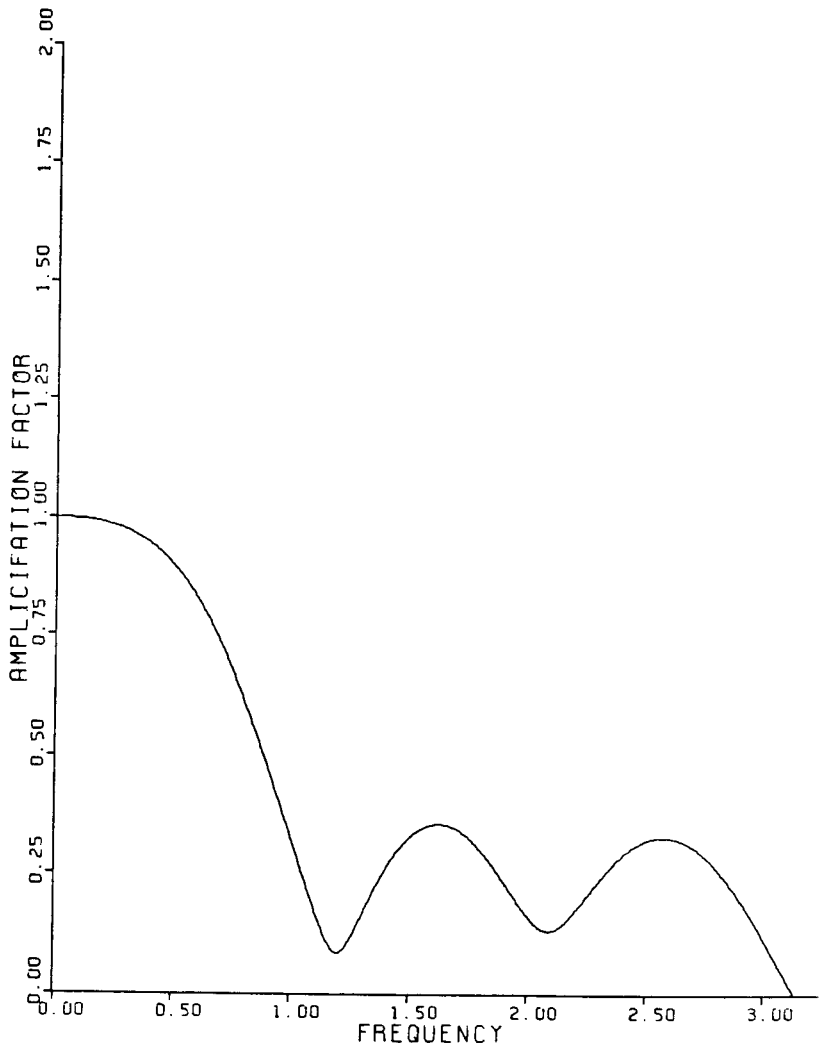

Figure 7: Amplification Factor $|g|$ of Standard 4 Stage with Single Evaluation of Dissipation and Modified Coefficients for $\lambda = 2, \mu = 1/32$ Coefficients of $\alpha_1 = .25, \alpha_2 = .5, \alpha_3 = .55$

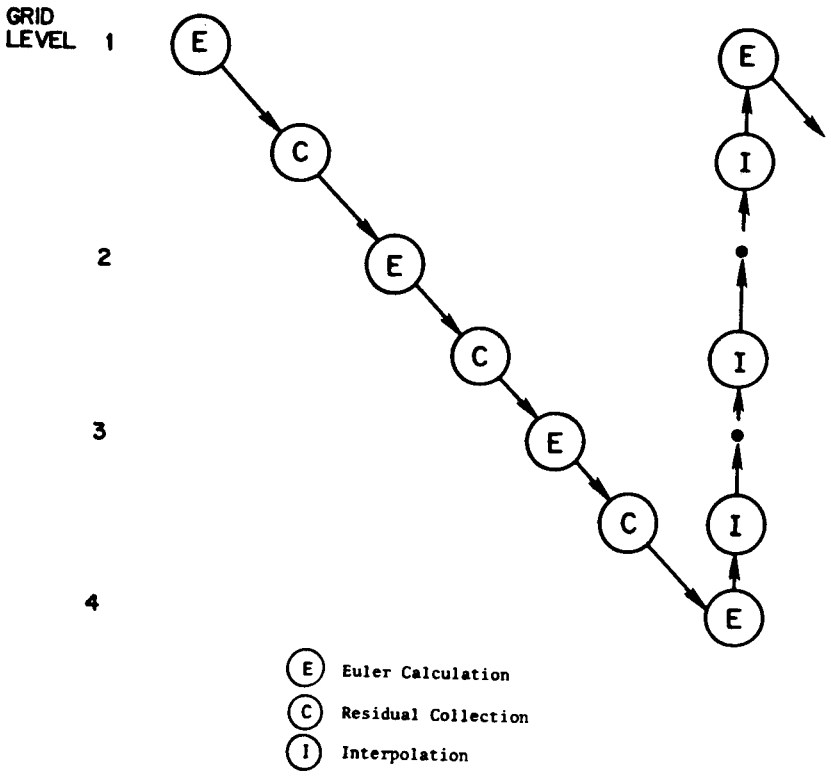

Figure 8: Saw Tooth Multigrid Cycle

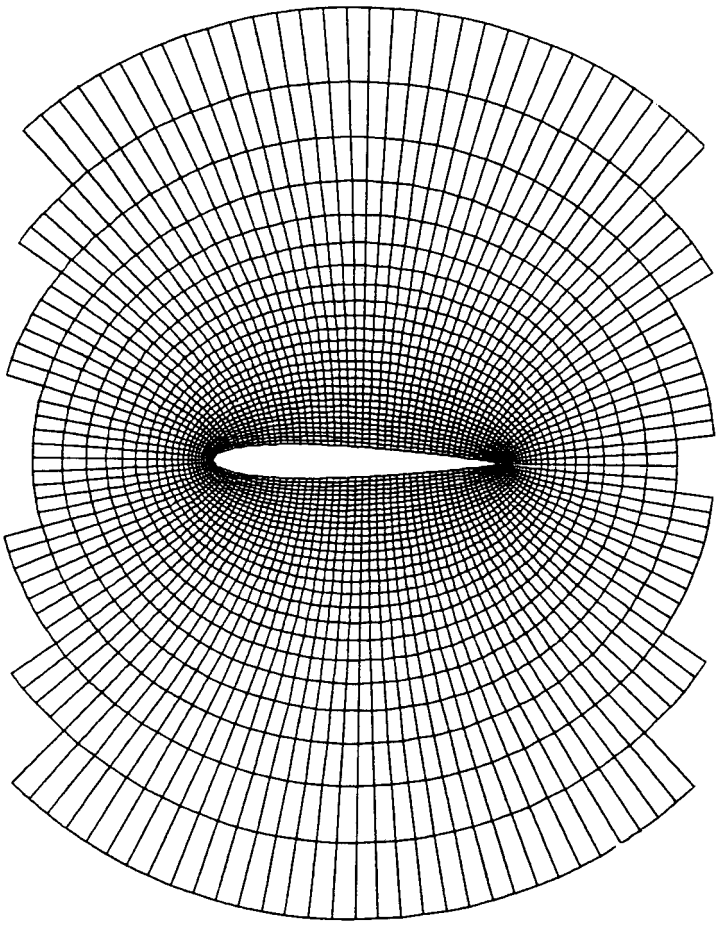

Figure 9: Grid for NACA 0012 128x32 cells

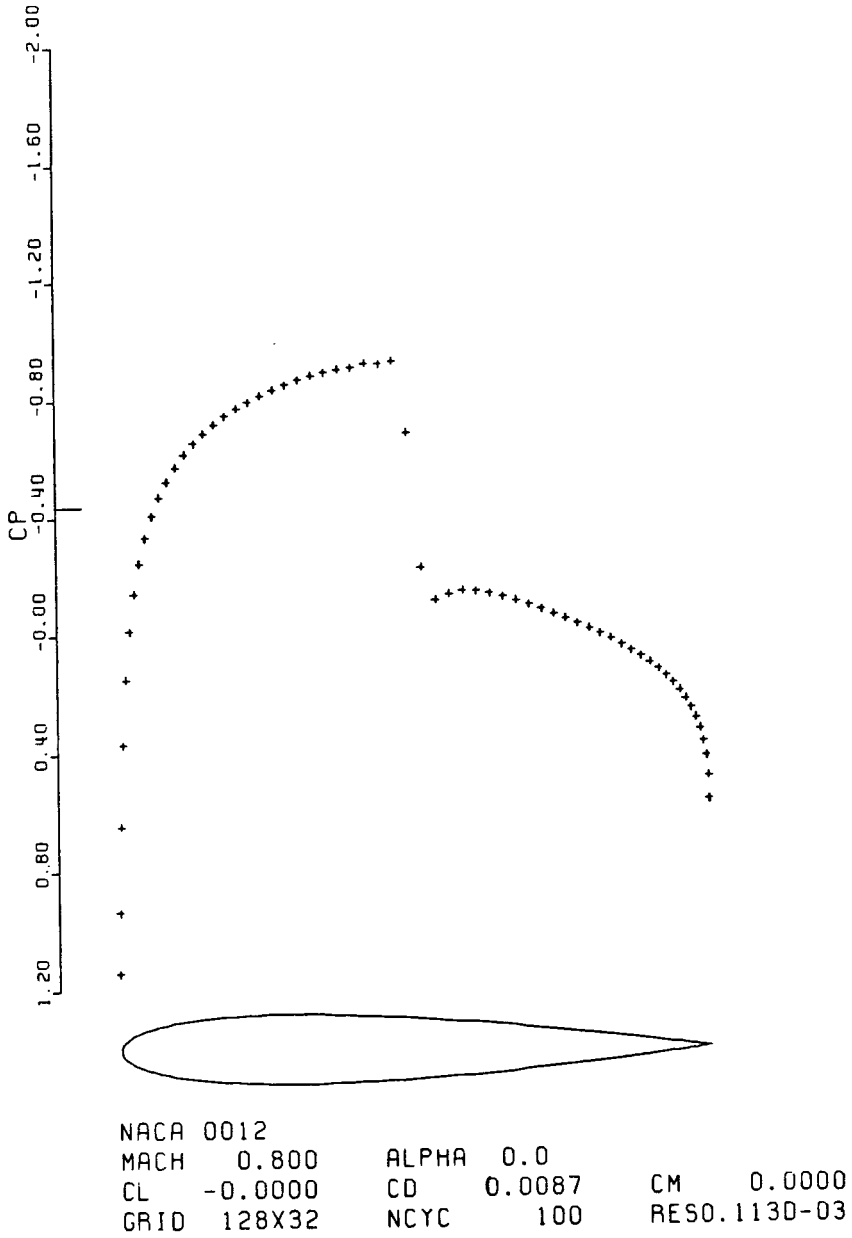
CP
-2.00
-1.60
-1.20
-0.80
-0.40
-0.00
0.40
0.80
1.20
NACA 0012
MACH 0.800 ALPHA 0.0
CL -0.0000 CD 0.0087 CM 0.0000
GRID 128X32 NCYC 100 RESO.113D-03

Figure 10:

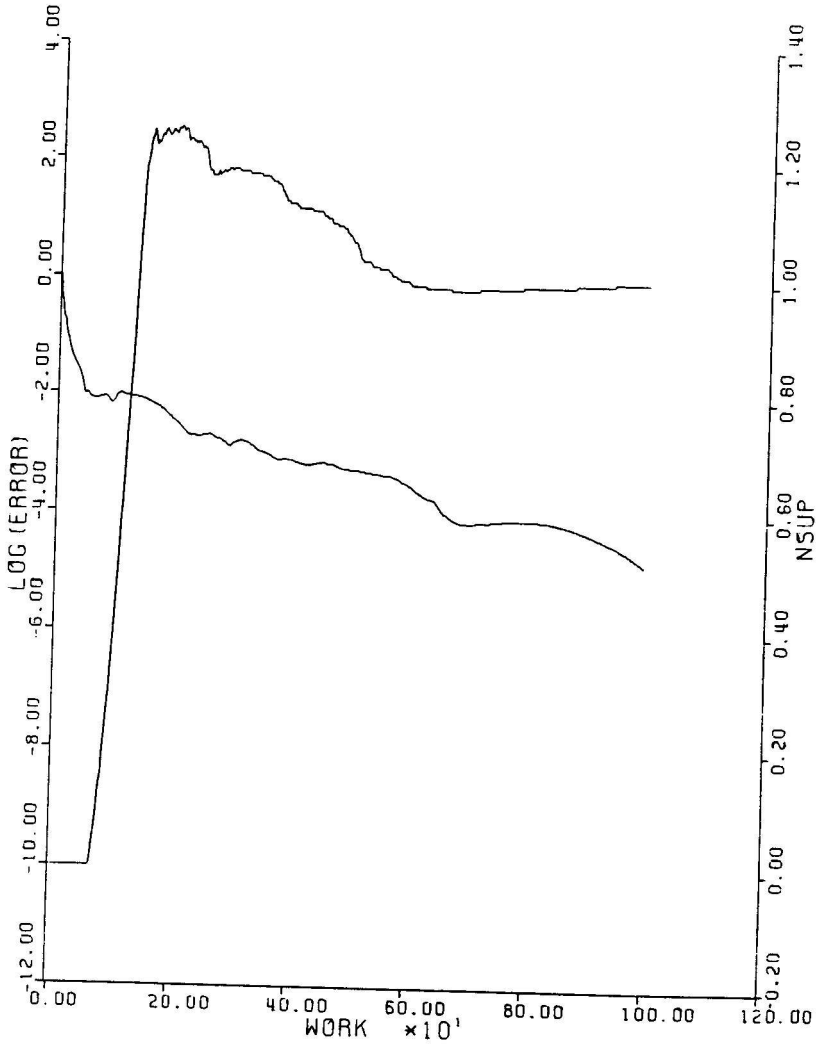
LOG (ERROR)
4.00
2.00
0.00
-2.00
-4.00
-6.00
-8.00
-10.00
-12.00
0.00
20.00
40.00
60.00
80.00
100.00
120.00
WORK ×10¹
NSUP
1.40
1.20
1.00
0.80
0.60
0.40
0.20
0.00
-0.20
NACA 0012
MACH 0.800
ALPHA 0.0
RESID1 0.341D+01
RESID2 0.510D-04
WORK 998.00
RATE 0.9889
GRID 128X32

Figure 11:

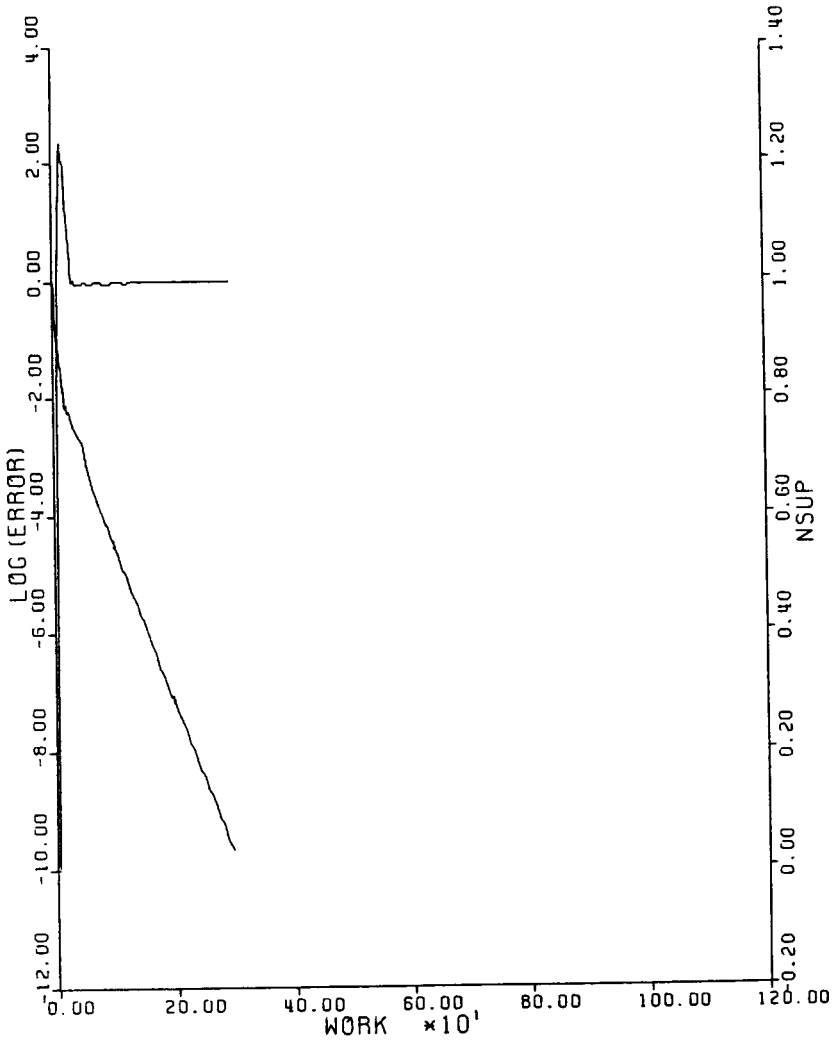

NACA 0012

MACH	0.800	ALPHA	0.0
RESID1	0.329D+01	RESID2	0.689D-09
WORK	299.00	RATE	0.9282
GRID	128X32		

Figure 12:

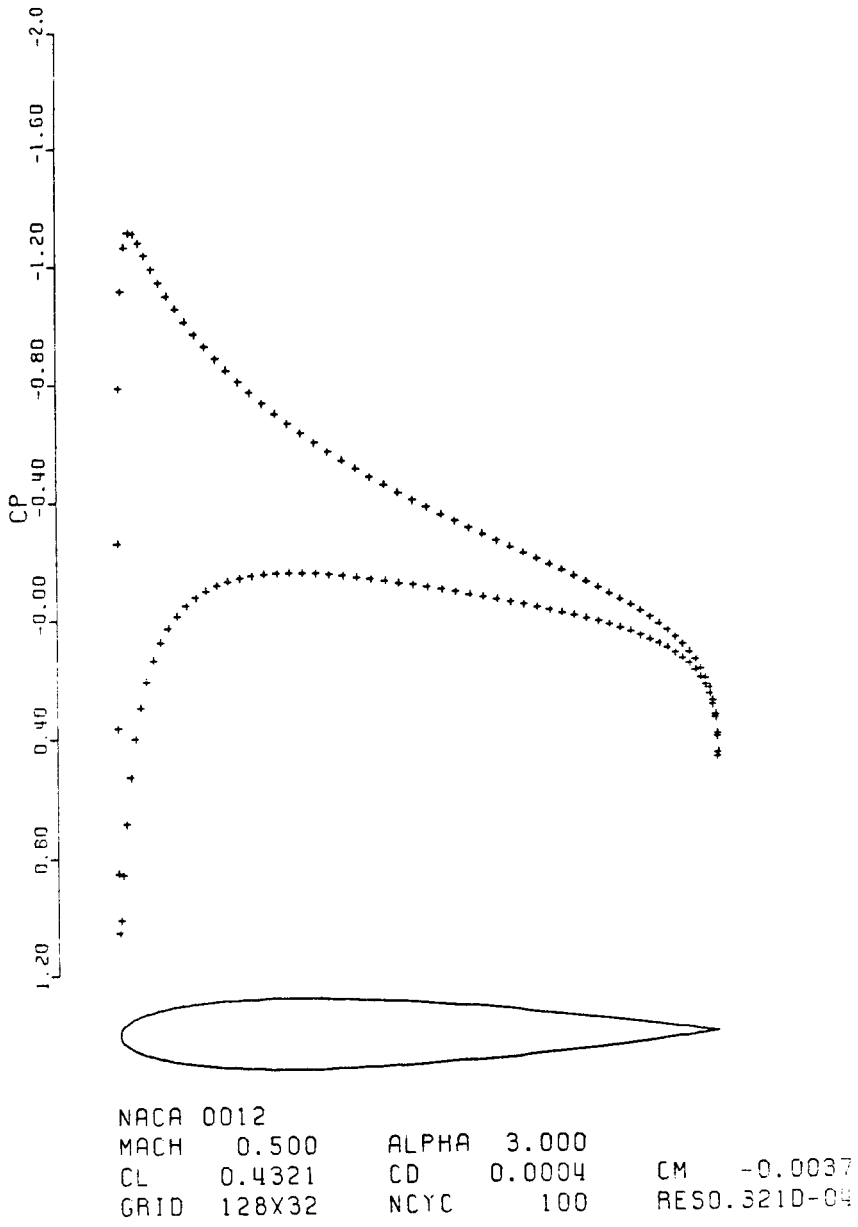
CP
-2.0
-1.60
-1.20
-0.80
-0.40
-0.00
0.40
0.80
1.20
NACA 0012
MACH 0.500 ALPHA 3.000
CL 0.4321 CD 0.0004 CM -0.0037
GRID 128X32 NCYC 100 RESO.321D-04

Figure 13:

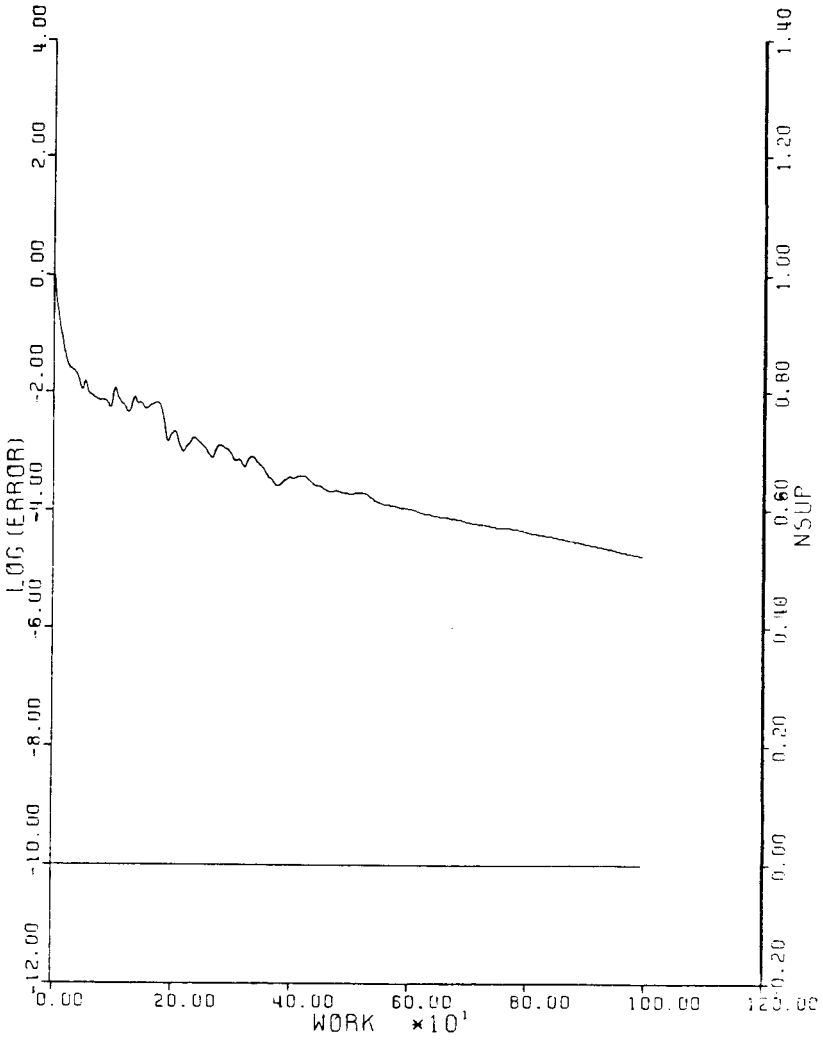
LOG (ERROR)
4.00
2.00
0.00
-2.00
-4.00
-6.00
-8.00
-10.00
-12.00
0.00
20.00
40.00
60.00
80.00
100.00
WORK ×10¹
1.40
1.20
1.00
0.80
0.60
0.40
0.20
0.00
NSUP
NACA 0012
MACH 0.500
ALPHA 3.000
RESID1 0.200D+01
RESID2 0.328D-04
WORK 998.00
RATE 0.9890
GRID 128X32

Figure 14:

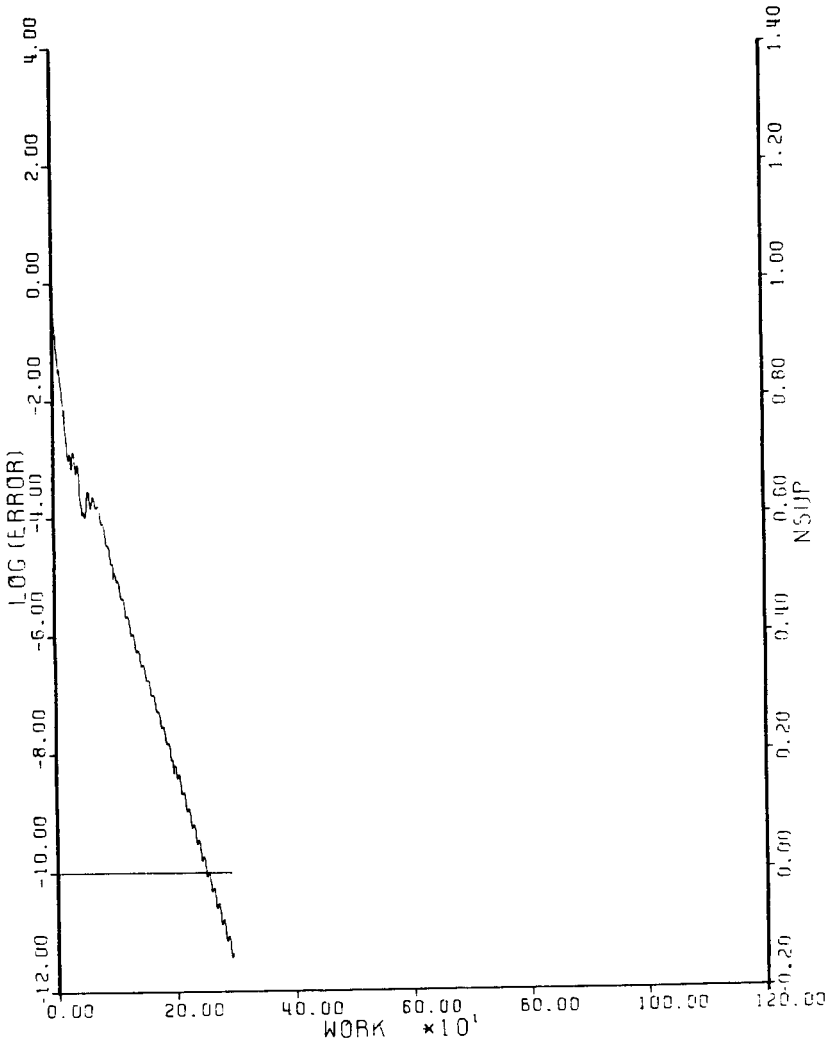

NACA 0012			
MACH	0.500	ALPHA	3.000
RESID1	0.196D+01	RESID2	0.8500-11
WORK	299.00	RATE	0.9102
GRID	128X32		

Figure 15:

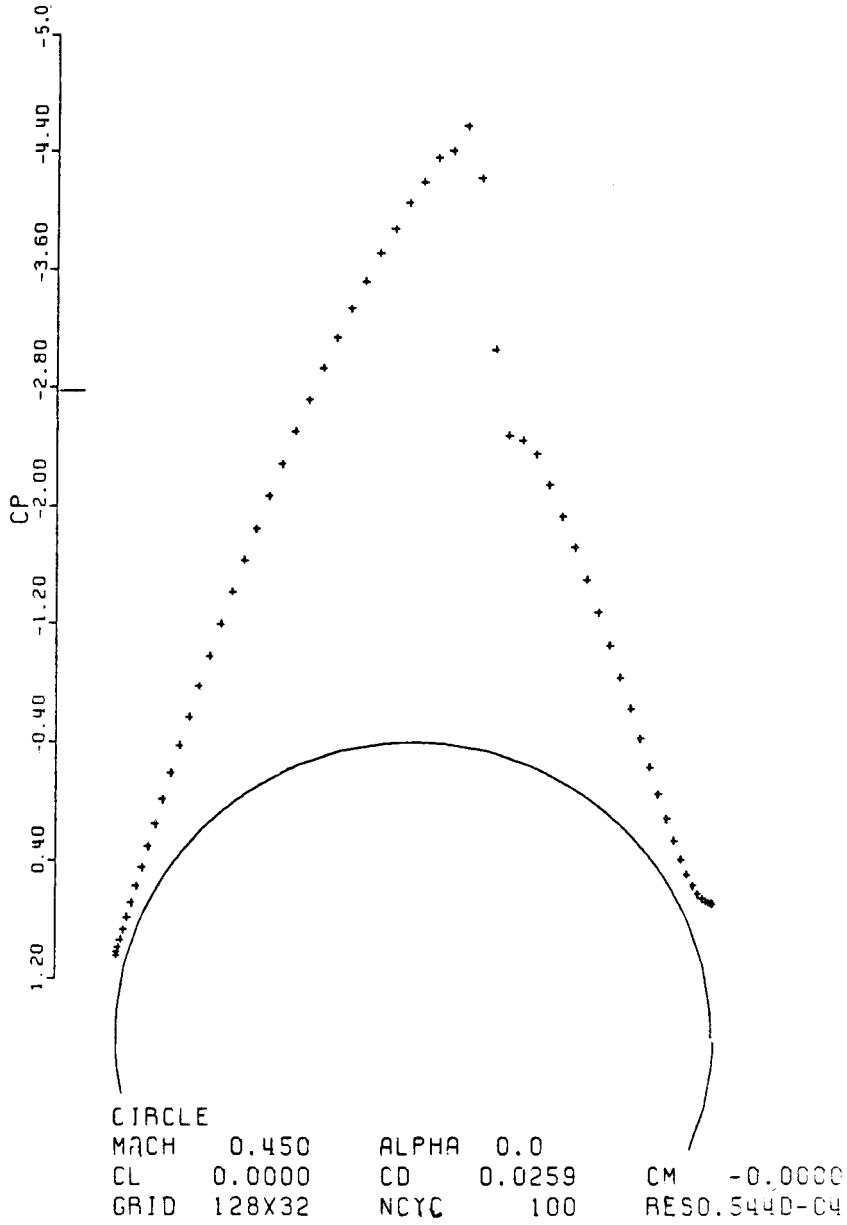
CP
-5.0
-4.40
-3.60
-2.80
-2.00
-1.20
-0.40
0.40
1.20
CIRCLE
MACH 0.450 ALPHA 0.0
CL 0.0000 CD 0.0259 CM -0.0000
GRID 128X32 NCYC 100 RESD.5440-04

Figure 16:

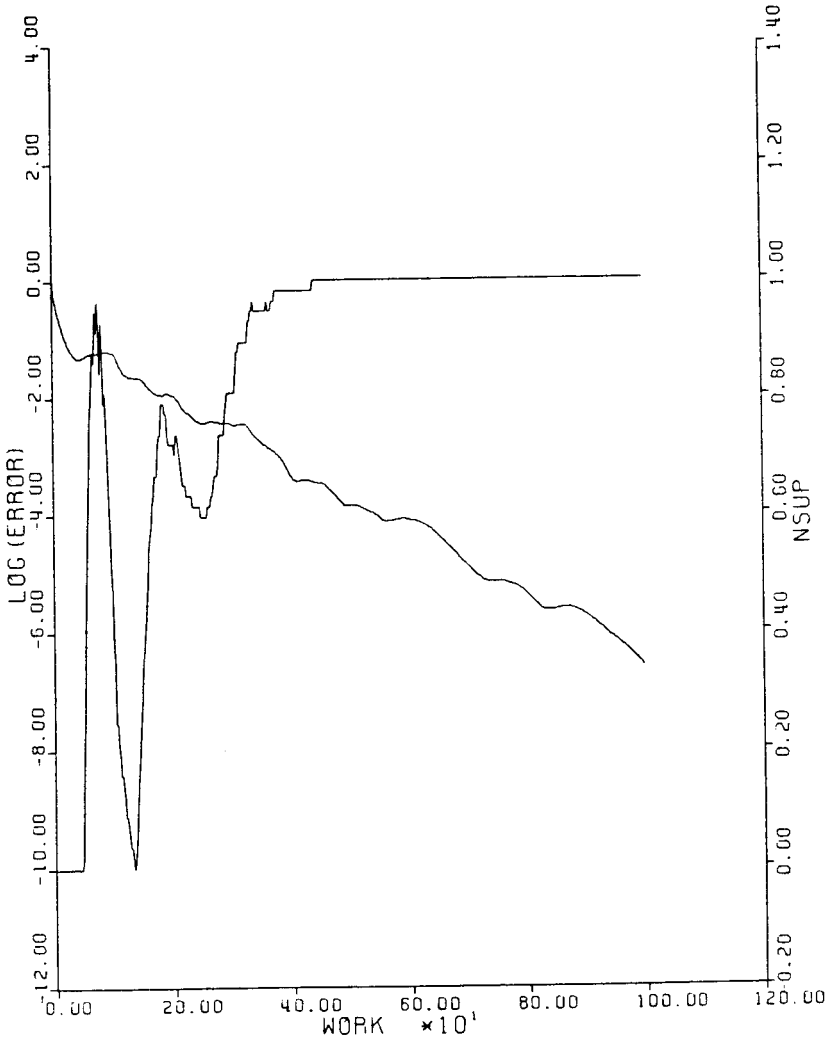

CIRCLE			
MACH	0.450	ALPHA	0.0
RESID1	0.184D+01	RESID2	0.471D-06
WORK	998.00	RATE	0.9849
GRID	128X32		

Figure 17:

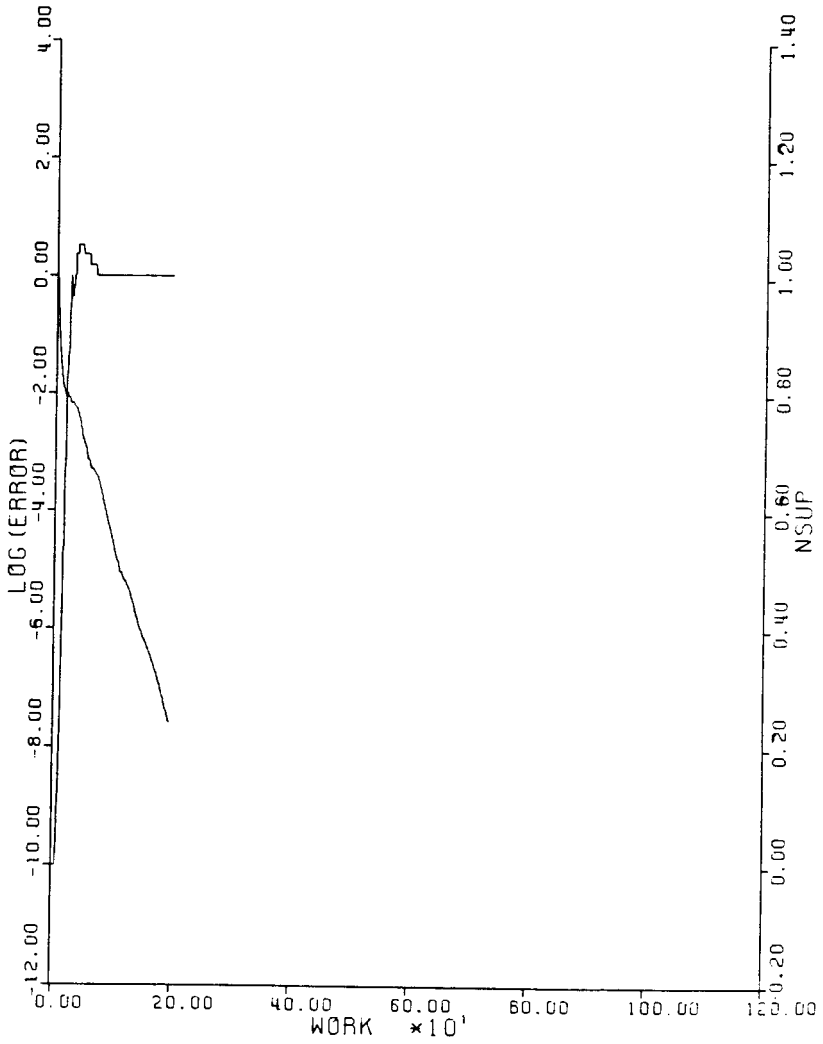

CIRCLE			
MACH	0.450	ALPHA	0.0
RESID1	0.182D+01	RESID2	0.470D-07
WORK	199.00	RATE	0.9159
GRID	128X32		

Figure 18: